COLORIMETRIC DETECTION OF Fe(II) and Co(II) BY USING TERPYRIDINE-BASED DERIVATIVE**

Xiaobo Wang [1], Yongpeng Ma [2], Zhenxing Li [2], Guanglu Han [2], Xidong Guan [3*], Kaiqi Fan [2*]

[1] Journal Editorial Department, Zhengzhou University of Light Industry, Zhengzhou, China
[2] School of Material and Chemical Engineering at Zhengzhou University of Light Industry, Zhengzhou, China; e-mail: benlto@163.com
[3] School of Pharmaceutical Sciences at Shandong First Medical University & Shandong Academy of Medical Sciences, Taian, China; e-mail: xidongguan@163.com

A multi-ion chromogenic sensor based on a terpyridine moiety was developed for the semiquantitative, visual, and sensitive speciation analysis of Fe^{2+} and Co^{2+} ions in water. Each metal ion exhibited a different color, and significant color evolution was observed by the naked eye, resulting in semiquantitative visual detection. A smartphone was used for visual detection by identifying the RGB values of the probe solutions. The application of smartphones shortened the detection time dramatically and reduced the detection cost. This method provides a new strategy for the semiquantitative detection of heavy metal ions in water samples.

Keywords: *visual detection, RGB value, terpyridine-based derivative.*

КОЛОРИМЕТРИЧЕСКОЕ ОПРЕДЕЛЕНИЕ Fe(II) и Co(II) С ИСПОЛЬЗОВАНИЕМ ПРОИЗВОДНОГО ТЕРПИРИДИНА

X. Wang [1], Y. Ma [2], Zh. Li [2], G. Han [2], X. Guan [3*], K. Fan [2*]

УДК 543.42:546.3

[1] Университет легкой промышленности Чжэнчжоу, Чжэнчжоу, Китай
[2] Школа материаловедения и химической инженерии Университета легкой промышленности Чжэнчжоу, Чжэнчжоу, Китай; e-mail: benlto@163.com
[3] Школа фармацевтических наук Первого медицинского университета Шаньдуня и Академии медицинских наук Шаньдуня, Тайань, Китай; e-mail: xidongguan@163.com

(Поступила 25 мая 2021)

Разработан мультиионный хромогенный сенсор на основе терпиридинового фрагмента для полуколичественного, визуального и чувствительного анализа состава ионов Fe^{2+} и Co^{2+} в воде. Каждый ион металла имеет свой цвет, и невооруженным глазом наблюдается его значительная эволюция, что приводит к полуколичественному визуальному обнаружению. Для визуального обнаружения растворов зонда путем определения значений RGB использован смартфон. Показано, что применение смартфонов резко сокращает время обнаружения и снижает стоимость процедуры.

Ключевые слова: *визуальная детекция, значение RGB, производное на основе терпиридина.*

Introduction. Recently, the fast and inexpensive detection of heavy metals in water has become one of the most popular research domains owing to the rapid urbanization and industrialization, resulting in widespread environmental pollution [1–3]. Researchers have attempted subtle approaches to find selective and sensitive detection methods for toxic heavy metals [4, 5]. Heavy metal ions pose a serious threat to the environment and human health and have a variety of toxicities that can cause serious diseases and even death [6–9]. Among the various metal ions, Co^{2+} is an essential trace element for all animals [10, 11]. The lack

**Full text is published in JAS V. 89, No. 3 (http://springer.com/journal/10812) and in electronic version of ZhPS V. 89, No. 3 (http://www.elibrary.ru/title_about.asp?id=7318; sales@elibrary.ru).

of cobalt ions in the body can cause anemia and hypothyroidism, and increase the risk of infant developmental abnormalities and failure [12, 13]. On the other hand, the inorganic form of cobalt is highly toxic to humans, and excessive amounts of this metal can cause cobalt poisoning [14].

Iron is also essential for biological functions in the human body, where it exists as ferrous (Fe^{2+}) and ferric (Fe^{3+}) ions under physiological conditions [15, 16]. The appropriate concentration of iron ions is essential to health. The excessive accumulation of iron ions has serious consequences, including dysfunction of the vital organs, cancer, hemochromatosis, and hepatitis [17–19]. Moreover, Fe^{2+} is a potential catalyst of the Fenton reaction, which causes severe cellular damage by generating hydroxyl radicals, which are the most harmful active oxygen in biological systems [20]. Thus, the development of a sensor for detecting metal ions is a significant issue in both biological systems and the environment.

Various methods for detecting metal ions have been used, including chromatography, atomic absorption and emission spectroscopy, and electrochemical methods [21–23]. Unfortunately, most of these methods are expensive, time-consuming, and show insufficient sensitivity; therefore, it is necessary to design and synthesize highly sensitive and selective sensors for detecting heavy metal ions. Chromogenic sensors overcome these limitations and are very useful for naked-eye monitoring of metal ions, owing to their sensitivity, reliability, and visualization [24–27], for example, Nawaz et al. reported a sensor containing phenanthroline for the instant naked-eye detection of Fe^{2+} ions [28], while Liu et al. reported a fluorescent carbon dot sensor for the semiquantitative assay of Cu^{2+} by a dose-sensitive color evolution [29], and Zhou et al. prepared a fluorescent test paper with a "from red to cyan" response to the presence and amount of arsenic ions [30]. Thus, a colorimetric method enables the sensitive, visible, simple, and low-cost detection of various metal ions.

In recent years, after installing the appropriate applications, smartphones have shown powerful functionality and have been used widely in various fields [31, 32]. The semiquantitative detection of metal ions can be achieved by combining a smartphone with colorimetric methods. Herein, a new multi-ion chromogenic sensor was synthesized by reacting 4′-(4-pyridyl)-2,2′:6′,2″-terpyridine with 3-bromopropene. The sensor was designed and used for the effective colorimetric detection of Fe^{2+} and Co^{2+} ions in water, and visual, real-time, and semiquantitative detection was achieved using a smartphone application.

Experimental. *Materials and methods.* All reagents, metal ions, and solvents were purchased from Aldrich chemical company. 4′-(4-Pyridyl)-2,2′:6′,2″-terpyridine was synthesized using a method reported elsewhere [14]. Distilled water was used throughout the study, and all chemicals were of analytical grade and used as received. The nuclear magnetic resonance (NMR) spectra were obtained on a Bruker DPX 400 MHz spectrometer using tetramethylsilane as an internal standard. The chemical shifts were reported as δ values (ppm) relative to the residual peak of the solvent. The mass spectra were recorded on a Thermo Fisher-Exactive Orbitrap mass spectrometer. UV-Vis spectroscopy was conducted on a Jasco V-570 UV/Vis/NIR spectrophotometer using a 1-cm quartz cell at 25°C. The Apple iPhone 6, using the color picker iOS application, was used.

Synthesis of 4′-(N-propenyl-4-pyridinio)-2,2′:6′,2″-terpyridine bromide (PPY). A mixture of 4′-(4-pyridyl)-2,2′:6′,2″-terpyridine (0.16 g, 0.52 mmol) and 3-bromopropene (0.242 g, 2 mmol) was added to acetonitrile (20 mL) under a N_2 atmosphere, and the solution was stirred under reflux for 24 h. After the mixture was cooled to room temperature, the resulting precipitate was filtered off and washed with acetonitrile. The final product was recrystallized from ethanol to obtain a white powder of PPY with a 91% yield.

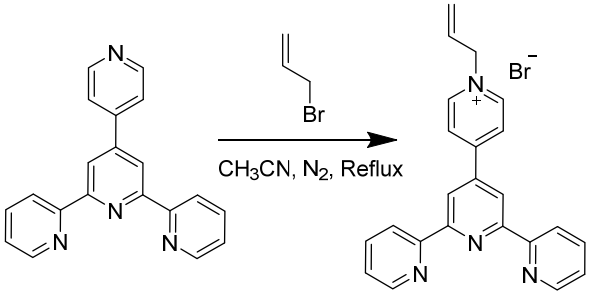

PPY

^{1}H NMR (400 MHz, DMSO-d_6, 298 K) δ (ppm): 9.19 (d, J = 6.8 Hz, 2H), 8.93 (s, 2H), 8.84–8.78 (m, 4H), 8.72 (d, J = 8.0 Hz, 2H), 8.10 (m, 2H), 7.60 (m, 2H), 6.23 (m, 1H), 5.50 (dd, J = 20.1, 9.7 Hz, 2H), 5.36 (d, J = 6.1 Hz, 2H). ^{13}C NMR (400 MHz, DMSO-d_6, 298 K) δ (ppm):156.82, 154.63, 153.49, 149.90, 145.86, 144.32, 138.23, 132.23, 126.57, 125.53, 122.34, 121.69, 119.26, 62.47. ESI-MS: $[C_{23}H_{19}N_4]^+$ 351.1610.

Results and discussion. The PPY probe was synthesized by reacting 4′-(4-pyridyl)-2,2′:6′,2″-terpyridine with 3-bromopropene under reflux in acetonitrile, which gave PPY in 90% yield. The synthesized probe was confirmed by and characterized by ^{1}H and ^{13}C NMR and electrospray ionization (ESI)-mass spectrometry. The probe with good water solubility prompted this investigation of the metal ion sensing properties of PPY in water systems.

Visual detection. The selectivity of PPY was determined by examining the naked-eye detectable color changes of PPY by adding one equivalent of various metal ions in aqueous media. The nitrate salts of Cd^{2+}, Zn^{2+}, Hg^{2+}, Fe^{2+}, Ca^{2+}, Co^{2+}, Pb^{2+}, Cu^{2+}, Mg^{2+}, Mn^{2+}, and Ni^{2+} were used to evaluate its metal-ion-sensing properties. The probe immediately changed its color from colorless to blue with Fe^{2+} and pink with Co^{2+}, whereas it did not show any color change in the presence of the other metal ions examined. The interaction of PPY with metal ions was examined by UV-Vis spectroscopy of PPY and its mixtures with various metal ions in an aqueous solution at room temperature. As shown in Fig. 1, after adding one equivalent of the Fe^{2+} and Co^{2+}, a new peak appeared in the absorption spectra of PPY (595 nm for Fe^{2+} and 540 nm for Co^{2+}), suggesting the formation of PPY-Fe^{2+} and PPY-Co^{2+} complexes [31, 32]. However, PPY did not show any noticeable responses to other metal ions, confirming the high selectivity and immediate response of PPY.

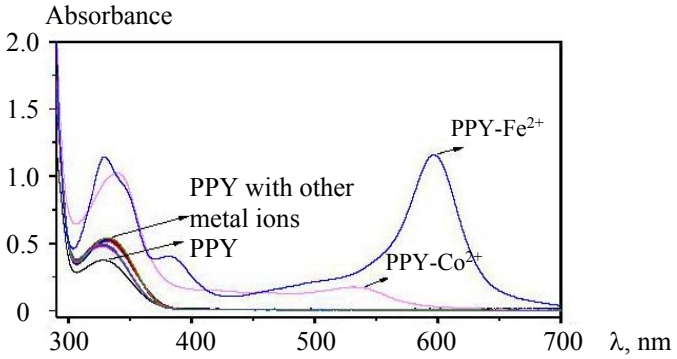

Fig. 1. UV-Vis spectral response of PPY (10 μM) with 1 eqv. of various metal ions.

Absorption spectral response. The sensitivity of PPY toward the metal ions (Fe^{2+} and Co^{2+}) was examined by UV-Vis titration experiments (Fig. 2). As shown in Fig. 2a, the sequential addition of Fe^{2+} ions to an aqueous solution of PPY resulted in an increase of the absorption bands at 327 and the appearance of a new band at 595 nm, thus indicating the presence of PPY-Fe^{2+} complexes in the solution. The band appeared at 595 nm because of metal-to-ligand charge transfer (MLCT) upon the formation of the PPY-Fe^{2+} complex [27]. The limit of detection (LOD) for Fe^{2+} was determined to be 6×10^{-7} M, based on $3\sigma/k$ [32], where σ is the standard deviation of the blank measurement, and k is the slope of the plot obtained by plotting the absorption versus the analyte concentration (Fig. 2a, inset). The binding stoichiometry of PPY with Fe^{2+} was further determined by Job plot analysis [30]. The change in absorbance at 595 nm was plotted as a function of the mole fraction of PPY under the constant total concentration. A maximum intensity appeared at the mole fraction of 0.5, which indicated a 1:1 binding mode between PPY and Fe^{2+} (Fig. 3a). Based on the titration measurement, the binding constant (K) of PPY with Fe^{2+} was calculated to be 5.9×10^{3} M^{-1} using the Benesi–Hildebrand equation (Fig. 3b) [31].

The UV-Vis titration of PPY toward Co^{2+} was carried out to understand the binding properties. Upon the addition of Co^{2+}, the UV-Vis absorption peak at 327 nm increased, and a new band appeared at 540 nm (Fig. 2b). The band at 540 nm was assigned to metal-to-ligand charge transfer (MLCT) upon the formation of a PPY-Co^{2+} complex. As shown in Fig. 2b (inset), the calculated limit of detection (LOD) of PPY for Co^{2+} was 8.8×10^{-6} M. Job plot analysis revealed 1:1 stoichiometry for PPY and Co^{2+} (Fig. 3c). The binding constant (K) for Co^{2+} was determined to be 9.0×10^{3} M^{-1} using the Benesi–Hildebrand equation (Fig. 3d).

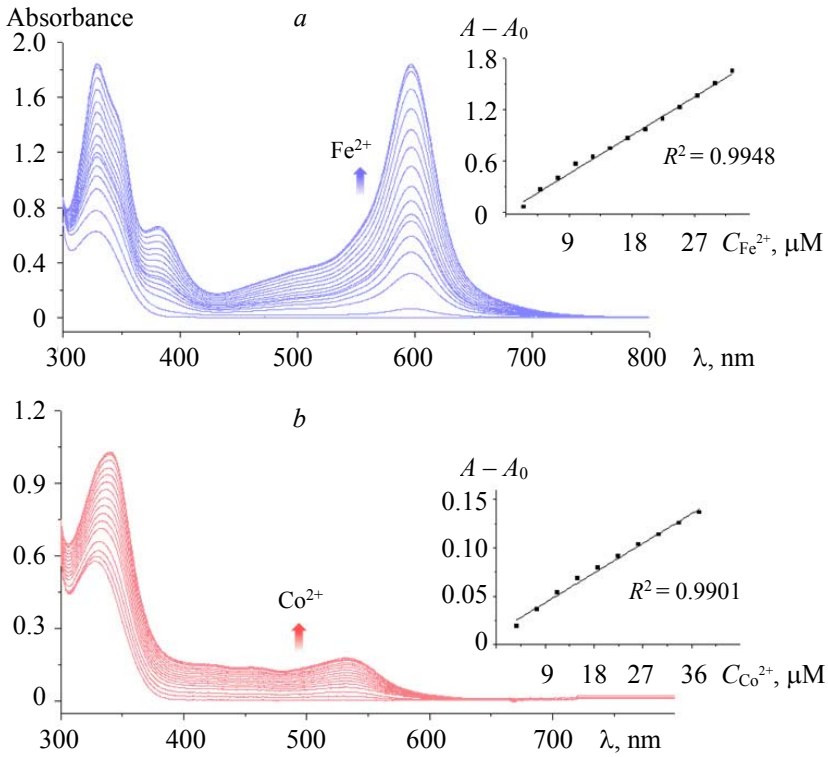

Fig. 2. a) UV-Vis absorption of PPY [50 μM] were recorded after adding Fe^{2+} ([Fe^{2+}] = 0, 2.5, 5.0, 7.5, 10.0, 12.5, 15.0, 17.5, 20.0, 22.5, 25.0, 27.5, 30.0, 32.5, 35.0, 37.5, and 40.0 μM), the inset shows the changes in absorbance at 595 nm vs. the Fe^{2+} concentration (A and A_0 are the absorbances at 595 nm in the presence and absence of Fe^{2+}, respectively). b) UV-Vis absorption of PPY [50 μM] were recorded after adding Co^{2+} ([Co^{2+}] = 0, 3.75, 7.50, 11.25, 15.00, 18.75, 22.50, 26.25, 30.00, 33.75, 37.50, 41.25, 45.00, 48.75, 52.50, 56.25, and 60.00 μM). The inset shows the changes in absorbance at 540 nm vs. the Co^{2+} concentration (A and A_0 are the absorbances at 540 nm in the presence and absence of Co^{2+}, respectively).

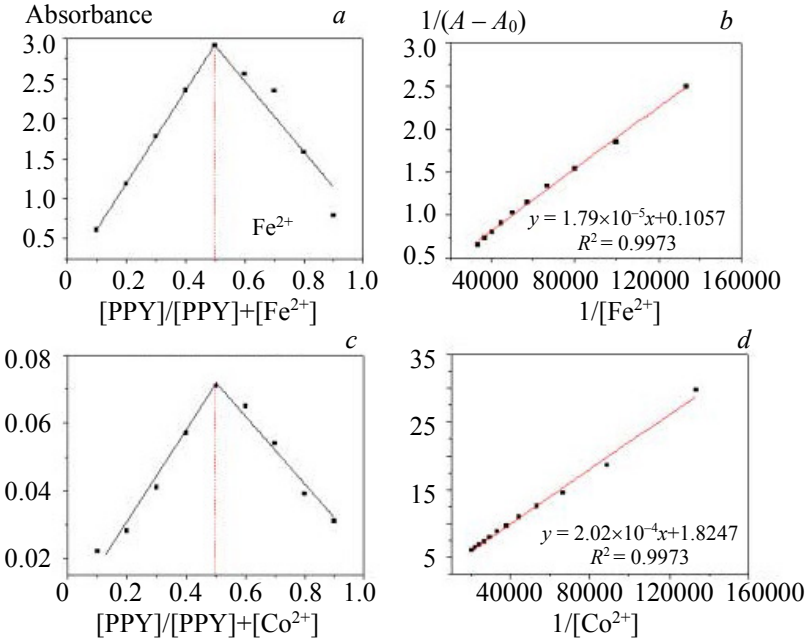

Fig. 3. Job plot for (a) PPY-Fe^{2+} and (c) PPY-Co^{2+} complex formation. BH plot for (b) PPY-Fe^{2+} and (d) PPY Co^{2+} complex.

Mechanism of binding. The binding mechanism of PPY for the metal ions was confirmed by taking the mass spectrum of the probe with each metal ion. Fourier transform mass spectrometry (FTMS) of the PPY probe revealed an intense peak at *m*/*z* 351.16, corresponding to the probe moiety (Fig. 4). After adding Fe^{2+}, the probe solution mass was recorded at *m*/*z* 234.57, which was assignable to PPY–Br^{-}+Fe^{2+}+NO_3^{-} [calc. *m*/*z*: 234.54]. In addition, mass analysis also revealed a 1:1 binding stoichiometry between PPY and Fe^{2+} (Fig. 4a). Similarly, when Co^{2+} ions were added, the mass data of PPY for Co^{2+} revealed an intense peak at *m*/*z* 236.04 that was assigned to PPY−Br^{-}+Co^{2+}+NO_3^{-} [calc, *m*/*z*: 236.04]. The stoichiometric ratio between PPY and Co^{2+} was also 1:1 (Fig. 4b).

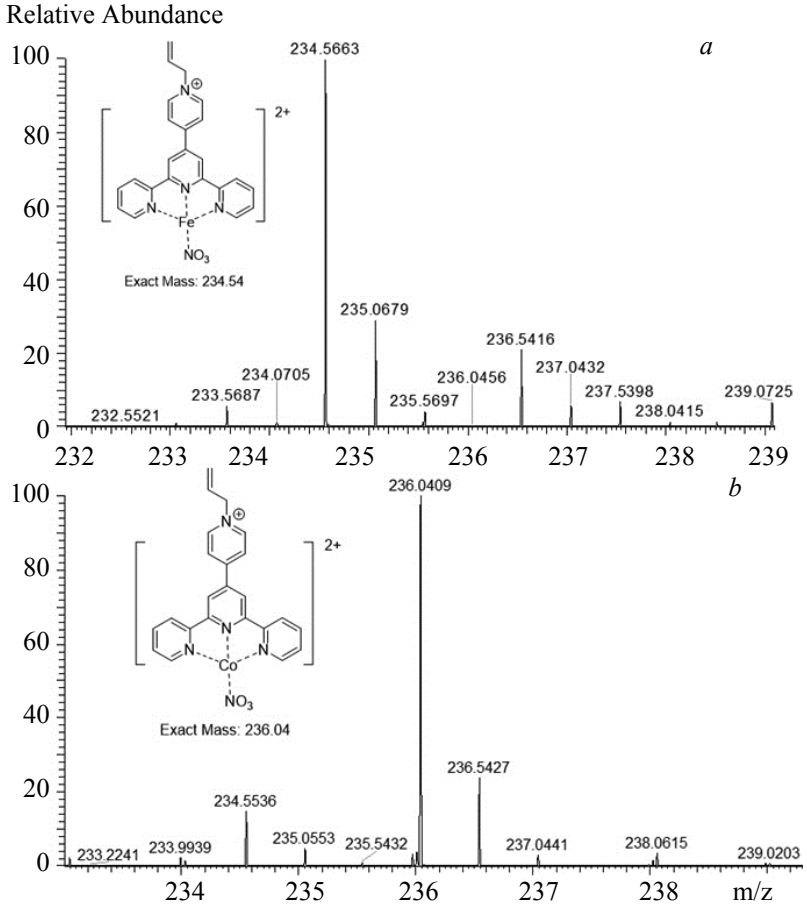

Fig. 4. Fourier transform mass spectra of (a) PPY-Fe^{2+} and (b) PPY-Co^{2+}.

RGB application. The capabilities of the probe for more accurate sensing were assessed by integrating the colorimetry chemosensor with a smartphone to examine the relationship between the color change and the concentrations of the two metal ions [33]. First, metal ion solutions with different concentrations (0–50 μM) were added, and photographs were taken with a smartphone. The color information (RGB values) of the probe was obtained using the smartphone application, Color Picker. The red and green channels were selected to calculate the RGB ratio of the red and green channels. The results showed a good linear relationship between the RGB ratio and the concentration of metal ions (Figs. 5a,b), and the calculated LODs were 0.18 μM for Fe^{2+} and 1.04 μM for Co^{2+}, respectively. Therefore, more accurate semiquantitative analysis can be achieved using a smartphone (Fig. 5c).

Analytical applications of PPY were performed using two different samples (local lake water and tap water) using the spike method. The quantitative analysis for each sample was carried out in three measurements. The recovery rates based on the UV-Vis spectral method and the RGB method were 96.53–99.16% and 96.44–102.73%, respectively (Table 1); hence, the colorimetric probe could detect Fe^{2+} and Co^{2+} effectively and reliably in actual water samples.

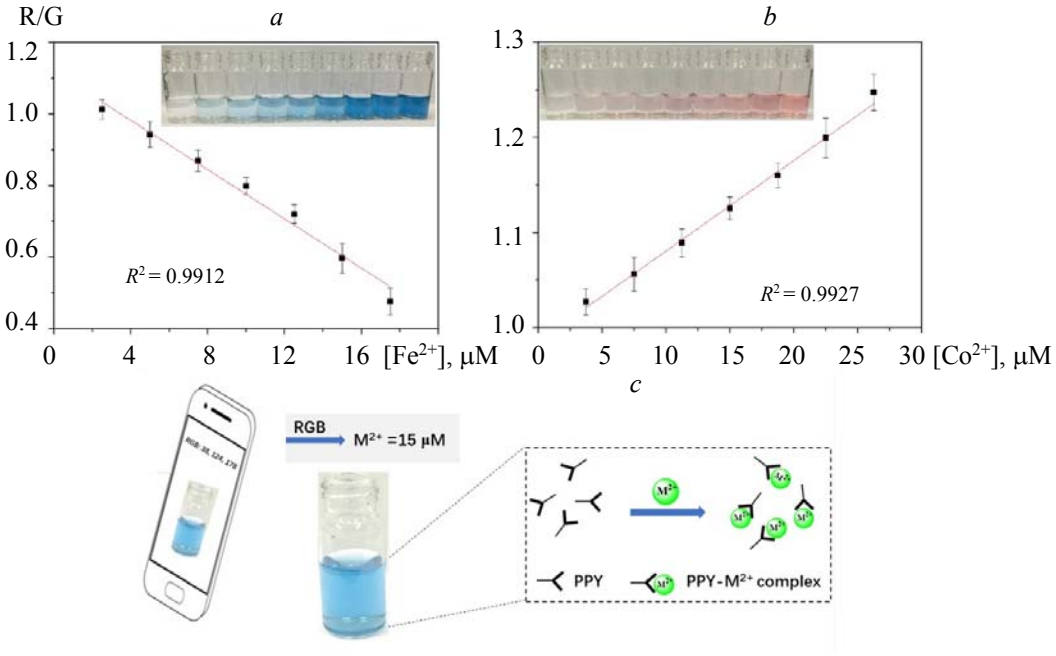

Fig. 5. Plot of PPY solution color change (red channel/green channel) as function of the concentration of a Fe^{2+} (a) and Co^{2+} (b) (the insets show photographs taken using a smartphone). Schematic drawing for the detection of metal ions using a smartphone (c). For all data points, $n = 3$.

TABLE 1. Performance of UV-Vis Spectral Method and RGB Method Towards Analysis of Fe^{2+} and Co^{2+} in Various Environmental Samples Using PPY

Water samples	Added, μM	UV-Vis spectral method		RGB method	
		Found, μM	Recovery, %	Found, μM	Recovery, %
Fe^{2+}					
Deionized water	4	3.92	98.05	3.95	98.69
	8	7.85	98.16	8.02	100.24
	12	11.73	97.74	11.92	99.31
	16	15.67	97.93	16.30	101.85
Tap water	4	3.93	98.15	3.95	98.77
	8	7.84	97.96	8.08	100.97
	12	11.79	98.22	11.64	97.03
	16	15.48	96.73	15.96	99.75
Lake water	4	3.88	97.05	3.91	97.69
	8	7.90	98.76	7.72	96.55
	12	11.74	97.84	12.18	101.46
	16	15.44	96.53	15.65	97.83
Co^{2+}					
Deionized water	5	4.85	97.03	4.92	98.37
	10	9.81	98.1	10.09	100.87
	15	14.65	97.69	14.70	98.02
	20	19.37	96.85	20.29	101.47
Tap water	5	4.86	97.15	4.88	97.57
	10	9.89	98.89	9.97	99.65
	15	14.87	99.16	15.41	102.73
	20	19.53	97.65	19.67	98.36
Lake water	5	4.85	96.97	4.92	98.34
	10	9.76	97.64	9.73	97.33
	15	14.81	98.72	15.02	100.14
	20	19.50	97.51	19.29	96.44

Conclusions. A highly selective chromogenic sensor with a terpyridine moiety that acts as a chelating site for metal ions was developed. PPY shows selective color changes from colorless to blue with Fe^{2+} and pink with Co^{2+} in an aqueous solution. The two metal ions were assigned to the terpyridine moiety of the probe molecule, which was confirmed by Job plot and mass spectrometry. The color RGB value of the probe solution could be identified using a smartphone application, which provided a simple visual analysis without the need for other instruments. In addition, the detection method with a smartphone application was applied to estimate the Fe^{2+} and Co^{2+} concentrations in real-time samples. Therefore, this approach can be applied to the fast recognition and discrimination of multi-ion analysis simultaneously in qualitative and semiquantitative manners without requiring complex statistical analysis.

Acknowledgments. This research was supported by the National Natural Science Foundation of China (21606211), Foundation of Henan Educational Committee (21A530009), Henan Provincial Natural Science Foundation (202300410502), Space Star Incubation Project (2019ZCKJ212), Shandong Provincial Natural Science Foundation (ZR2017BB019), Scientific Research Foundation for the Doctoral Program (2014BSJJ061).

REFERENCES

1. O. M. Acar, O. M. Kalfa, O. Yalcinkaya, A. R. Turker, *Anal. Methods*, **5**, 748–754 (2013).
2. M. D. Ioannidou, G. A. Zachariadis, A. N. Anthemidis, J. A. Stratis, *Talanta*, **65**, 92–97 (2005).
3. K. Fan, X. Wang, Y. Ma, Y. Li, G. Han, Z. Yin, J. Song, *RSC Adv*., **9**, 32137–32140 (2019).
4. J. Qi, B. Li, X. Wang, L. Fu, L. Luo, L. Chen, *Anal. Chem*., **90**, 11827–11834 (2018).
5. G. Heo, R. Manivannan, H. Kim, M. J. Kim, K. S. Min, Y.-A. Son, *Sens. Actuat. B*, **297**, 126723 (2019).
6. Y. Zhou, X. Huang, C. Liu, R. Zhang, X. Gu, G. Guan, C. Jiang, L. Zhang, S. Du, B. Liu, M.-Y. Han, Z. Zhang, *Anal. Chem*., **88**, 6105–6109 (2016).
7. K. Fan, X. Wang, Z. Yin, C. Jia, B. Zhang, L. Zhou, J. Song, *J. Mater. Chem. C*, **6**, 10192–10196 (2018).
8. A. W. Martinez, S. T. Phillips, E. Carrilho, S. W. Thomas, H. Sindi, G. M. Whitesides, *Anal. Chem*., **80**, 3699–3707 (2008).
9. X. Guan, K. Fan, T. Gao, A. Ma, B. Zhang, J. Song, *Chem. Commun*., **52**, 962–965 (2016).
10. Z. Liu, X. Jia, P. Bian, Z. Ma, *Analyst*, **139**, 585–588 (2014).
11. A. Maiga, D. Diallo, R. Bye, B. S. Paulsen, *J. Agric. Food Chem*., **53**, 2316–2321 (2005).
12. V. Battaglia, A. Compagnone, A. Bandino, M. Bragadin, C. A. Rossi, F. Zanetti, S. Colombatto, M. A. Grillo, A. Toninello, *Int. J. Biochem. Cell Biol*., **41**, 586–594 (2009).
13. K. Czarnek, S. Terpiłowska, A. K. Siwicki, *J. Immunol.*, **40**, 236–242 (2015).
14. Z. Zhang, J. Zhang, T. Lou, D. Pan, L. Chen, C. Qu, Z. Chen, *Analyst*, **137**, 400–405 (2012).
15. D. W. Domaille, E. L. Que, C. J. Chang, *Nat. Chem. Biol*., **4**, 168–175 (2008).
16. H. Weizman, O. Ardon, B. Mester, J. Libman, O. Dwir, Y. Hadar, Y. Chen, A. Shanzer, *J. Am. Chem. Soc*., **118**, 12368–12375 (1996).
17. C. Brugnara, *Clin. Chem*., **49**, 1573–1578 (2003).
18. X. B. Zhang, G. Cheng, W. J. Zhang, G. L. Shen, R. Q. Yu, *Talanta*, **71**, 171–177 (2007).
19. C. Qin, Y. Cheng L. Wang, X. Jing, F. Wang, *Macromolecules*, **41**, 7798–7804 (2008).
20. D. Galaris, V. Skiada, A. Barbouti, *Cancer Lett*., **266**, 21–29 (2008).
21. S. K. Sahoo, D. Sharma, R. K. Bera, G. Crisponi, J. F. Callan, *Chem. Soc. Rev*., **41**, 7195–7227 (2012).
22. K. Fan, X. Wang, H. Yang, L. Gao, G. Han, L. Zhou, S. Fang, *Anal. Methods*, **12**, 1561–1566 (2020).
23. J. X. Shi, C. Lu, D. Yan, L. Ma, *Biosens. Bioelectron*., **45**, 58–64 (2013).
24. S. M. Kang, S. C. Jang, G. Y. Kim, C. S. Lee, Y. S. Huh, C. Roh, *Sensors*, **16**, 626–636 (2016).
25. K. Fan, H. Kong, X. Wang, X. Yang, J. Song, *RSC Adv*., **6**, 80934–80938 (2016).
26. Y. W. Choi, G. J. Park, Y. J. Na, H. Y. Jo, S. A. Lee, G. R. You, C. Kim, *Sens. Actuators B*, **194**, 343–352 (2014).
27. K. Fan, X. Wang, S. Yu, G. Han, D. Xu, L. Zhou, J. Song, *Polym. Chem*., **10**, 5037–5043 (2019).
28. H. Nawaz, W. Tian, J. Zhang, R. Jia, Z. Chen, J. Zhang, C.-B. Sensor, *ACS Appl. Mater. Interfaces*, **10**, 2114–2121 (2018).
29. C. Liu, D. Ning, C. Zhang, Z. Liu, R. Zhang, J. Zhao, T. Zhao, B. Liu, Z. Zhang, *ACS Appl. Mater. Interfaces*, **9**, 18897–18903 (2017).
30. S. K. A. Kumar, K. Vijayakrishna, A. Sivaramakrishna, C. V. S. Brahmmananda Rao, N. Sivaraman, S. K. Sahoo, *Inorg. Chem*., **57**, 15270–15279 (2018).
31. H. Wang, L. Yang, S. Chu, B. Liu, Q. Zhang, L. Zou, S. Yu, C. Jiang, *Anal. Chem*., **91**, 9292–9299 (2019).
32. I. J. Kim, M. Ramalingam, Y. A. Son, *Sens. Actuat. B*, **246**, 319–326 (2017).
33. D. Gomez-Nicola, K. Riecken, B. Fehse, V. H. Perry, *Sci. Rep*., **4**, 7520 (2014).